Geophysical Research Letters

RESEARCH LETTER
10.1029/2024GL111782

Giant Undulations Driven by Pitch-Angle Scattering of Time Domain Structures Modulated by Plasmapause Surface Wave

Yi-Jia Zhou[1,2,3], Pei-Heng Du[4], Jian Liu[1,5], Quan-Qi Shi[6,7], Meng-Dan Guo[2,3], Fei He[2,3], Xiao-Xin Zhang[8], Yong-Liang Zhang[9], Zhong-Hua Yao[10], Jun Zhong[2,3], Zhaojin Rong[2,3], and Yong Wei[2,3]

[1]Weihai Institute for Interdisciplinary Research, Shandong University, Weihai, China, [2]Key Laboratory of Earth and Planetary Physics, Institute of Geology and Geophysics, Chinese Academy of Sciences, Beijing, China, [3]Colleage of Earth and Planetary Science, University of Chinese Academy of Sciences, Beijing, China, [4]North China Regional Air Traffic Management Bureau, CAAC, Beijing, China, [5]SDU-ANU Joint Science College, Shandong University, Weihai, China, [6]Laboratory of Optical Astronomy and Solar-Terrestrial Environment, School of Space Science and Physics, Institute of Space Sciences, Shandong University, Weihai, China, [7]State Key Laboratory of Space Weather, National Space Science Center (NSSC), Chinese Academy of Sciences, Beijing, China, [8]Key Laboratory of Space Weather, National Center for Space Weather, China Meteorological Administration, Beijing, China, [9]Johns Hopkins University Applied Physics Laboratory, Laurel, MD, USA, [10]NWU-HKU Joint Centre of Earth and Planetary Sciences, Department of Earth Sciences, University of Hong Kong, Hong Kong SAR, China

Abstract Plasmapause surface waves (PSWs) near the plasmapause boundary are regarded to be the magnetospheric source of ionospheric auroral giant undulations (GUs) located at the equatorward boundary of diffuse aurora. However, the observational evidence of wave-particle interaction connecting PSWs and GUs is absent. In this letter, we demonstrate GUs are driven by pitch-angle scattering of time domain structures modulated by the PSWs, based on the conjugated ionospheric and magnetospheric observations. Specifically, ionospheric GUs are lighted by the pitch-angle scattering of <1 keV thermal electron and ions and energetic ions with energy up to dozens of keV near the plasmapause. Further, the total fluxes during one PSW period and energy of scattered electron and ions determine the size and luminosity of GUs. Our research provides observational evidence that PSWs cause periodic electron precipitation via modulating the time domain structures rather than the previously predicted chorus or electron cyclotron harmonic waves.

Plain Language Summary Boundary surface waves usually act as a kind of special oscillation along the boundary layer and are the widely existing physical phenomena in the universe. In our Earth, there are magnetopause surface wave and plasmapause surface wave. For the latter, the plasmapause surface wave has been confirmed to be a kind of sawtooth-type auroral structures locating on the equatorial edge of aurora oval, named as giant undulations. But how can the plasmapause surface wave produce the auroral giant undulations is still unknown. Based on this question, we have provided the observational evidence of auroral giant undulations being driven by the periodic pitch-angle scattering of time domain structures modulated by plasmapause surface waves. Our new results in this research would help us to better understand the energy conversion controlled by boundary dynamics and the crucial effect of boundary dynamics on the near-surface space environment.

Key Points:

- Giant undulations (GUs) are lighted by the pitch-angle scattering of <1 keV thermal electron and ions and energetic ions with energy up to dozens of keV
- Total fluxes during one plasmapause surface wave (PSW) period and energy of scattered electron and ions determine the size and luminosity of GUs
- PSWs can cause periodic electron precipitation by modulating time domain structures

Correspondence to:
F. He,
hefei@mail.iggcas.ac.cn

Citation:
Zhou, Y.-J., Du, P.-H., Liu, J., Shi, Q.-Q., Guo, M.-D., He, F., et al. (2025). Giant undulations driven by pitch-angle scattering of time domain structures modulated by plasmapause surface wave. *Geophysical Research Letters*, *52*, e2024GL111782. https://doi.org/10.1029/2024GL111782

Received 2 AUG 2024
Accepted 29 JAN 2025

Author Contributions:
Conceptualization: Yi-Jia Zhou
Data curation: Yi-Jia Zhou, Fei He
Formal analysis: Yi-Jia Zhou
Funding acquisition: Fei He, Xiao-Xin Zhang
Investigation: Yi-Jia Zhou
Methodology: Yi-Jia Zhou
Project administration: Fei He
Software: Yi-Jia Zhou
Supervision: Fei He
Validation: Fei He
Visualization: Yi-Jia Zhou, Meng-Dan Guo
Writing – original draft: Yi-Jia Zhou
Writing – review & editing: Pei-Heng Du, Jian Liu, Quan-Qi Shi, Meng-Dan Guo, Fei He, Xiao-Xin Zhang, Yong-Liang Zhang, Zhong-Hua Yao, Jun Zhong, Zhaojin Rong, Yong Wei

1. Introduction

Boundary layer oscillations play a crucial role in energy, mass and moment conversion in the accretion disk (e.g., Stehle & Spruit, 1999), heliopause (e.g., Florinski et al., 2005), solar atmosphere (e.g., Li et al., 2013) and plasma tori surrounding planets (e.g., He et al., 2020; Xiao et al., 2023). In the terrestrial system, two kind of boundary oscillations from the outer to inner region manifest as the magnetopause surface eigenmode (MSE; e.g., Archer et al., 2019; Hartinger et al., 2015; Plaschke & Glassmeier, 2011) at the subsolar sector and Kelvin-Helmholtz (K-H) wave (e.g., Hasegawa et al., 2004; Li et al., 2023; Pu & Kivelson, 1983) at the flank sector on the magnetopause, and the plasmapause surface wave (PSW; e.g., Feng et al., 2023; He et al., 2020; Zhou, He, Archer, et al., 2024; Zhou et al., 2022) only observed at the dusk sector on the plasmapause. Based on theoretical predictions, numerical simulations and experimental observations (Archer et al., 2019; Chen & Hasegawa, 1974; Hartinger et al., 2015; He et al., 2020), the frequencies of the MSE and PSW both located at 0.5–2 mHz, typically

occupying the lower end of the ultra-low frequency (ULF; 0.1 mHz–1 Hz) waves. Therefore, such a kind of MSE and PSW with a global scale can certainly modulate the whole space weather environment and solar wind-magnetosphere-plasmasphere-ionosphere coupling efficiency.

The MSE can transport the solar wind energy deep into the inner magnetosphere via coupling with the global mode resonance and field line resonance (e.g., Agapitov et al., 2009; Mann et al., 1999; Rae et al., 2005; Zhou et al., 2023), while the PSW was observed to excite radially outward propagating ULF waves and subsequently trigger a similar filed line resonance phenomenon (He et al., 2020). Meanwhile, these magnetopause and plasmapause oscillations have been speculated to generate distinct aurora oscillations (e.g., Archer et al., 2023; Kozyreva et al., 2019) and giant undulations/sawtooth auroras (GUs/SAs; e.g., Lui et al., 1982) in the ionosphere, respectively. The GUs are a series of mesoscale sinusoidal or sawtooth aurora structures typically located at the equatorward boundary of diffuse aurora oval (e.g., Henderson et al., 2010; Lewis et al., 2005; Lui et al., 1982; Zhang et al., 2005; Zhou et al., 2021). Until recent years, based on the same morphology, azimuthal wavelength and sunward propagating velocity, He et al. (2020) have confirmed the GUs/SAs being the ionospheric manifestation of the magnetospheric PSW, which was generalized by the statistically consistency between the GUs and PSW (Feng et al., 2023; Zhou et al., 2021, 2022). Following it, Zhou, He, Archer, et al. (2024) revealed a four-region spatial evolution pattern of the PSW: seed, growth, stabilization and decay.

Limited by the rare opportunity of conjugate observation, however, the crucial intermediate physical processes bridging the PSW and GUs, especially the observational evidence of wave-particle interaction, remain absent. He et al. (2020) speculated that the periodic distribution of hot plasma modulated by PSW is probably scattered and precipitated by very low frequency (VLF) waves, like electron electrostatic cyclotron harmonic (ECH) or chorus waves. Subsequently in the same event, the PSW was observed to recurrently modulate the anti-correlated hiss and ECH waves (Hao et al., 2023). Neither of them concerned the pitch angle (PA) distribution of the PSW-modulated particles, which can directly determine the occurrence of ionospheric GUs or not. Noteworthy, a special particle precipitation pattern including energetic proton and low-energy electron precipitation above GUs was identified by Zhou, He, Zhang, et al. (2024), further hinting at the crucial particles distribution in the magnetospheric source. Therefore, in this letter, we are aiming to provide the direct observation evidence of wave-particle interaction connecting the PSW and GUs using the magnetospheric Van Allen Probe-A (VAP-A) and conjugated ionospheric Defense Meteorological Satellite Program (DMSP) F16, F17 and F19 satellites.

2. Results and Discussion

Low-earth-orbiting sun-synchronous DMSP F16, F17 and F19 and magnetospheric near-equatorial VAP-A are combined to conduct this research. The cross-track scanning aurora image in Lyman-Birge-Hopfield spectral band is from the Special Sensor Ultraviolet Spectrographic Imager (SSUSI) onboard DMSP (Paxton et al., 2002). The in situ wave and plasma data are obtained from the Electric and Magnetic Field Instrument Suite and Integrated Science (EMFISIS) (Kletzing et al., 2013), the Electric Field and Waves (EFW) (Wygant et al., 2013), the Helium, Oxygen, Proton, and Electron (HOPE) (Funsten et al., 2013) onboard VAP.

2.1. Ionospheric Observation of GUs

The selected event occurred at 16:00–21:00 UT on 7 September 2015, during which the magnetosphere suffered disturbance by a moderate geomagnetic storm with minimum *Dst* of −90 nT and multiple intense substorms of 800–2,800 nT for AE. Multiple DMSP satellites captured a long-lasting GUs event during 16:00–23:00 UT. Especially, the F17, F16 and F18 sequentially crossed the GUs at various magnetic local time (∼2 hr MLT) within several minutes (<4 min), approximately observing the simultaneous GUs at different MLT (i.e., wide-field GUs).

Figure 1 shows the aurora in the southern hemisphere at three specific moments in the uniform luminosity scale. For row 1, located at the equatorward boundary of equatorward expanding diffuse aurora, GUs have larger scales with amplitudes reaching up to ∼6° MLAT and higher aurora luminosity above 3 kilo-Rayleigh (kR), consideration of the antisunward bending of low-latitude crests of GUs (e.g., Lui et al., 1982; Nishitani et al., 1994). In row 2, only GUs with irregular wavelength and shape on the equatorward boundary of poleward shrinking aurora oval can be recognized with smaller latitudinal amplitudes all below 2° MLAT and lower aurora intensity less than 2 kR. In row 3, numerous GUs with latitudinal amplitudes reaching 6° MLAT and aurora luminosity more than 3 kR were again observed under the background of greatly equatorward expanding aurora oval. In brief, the

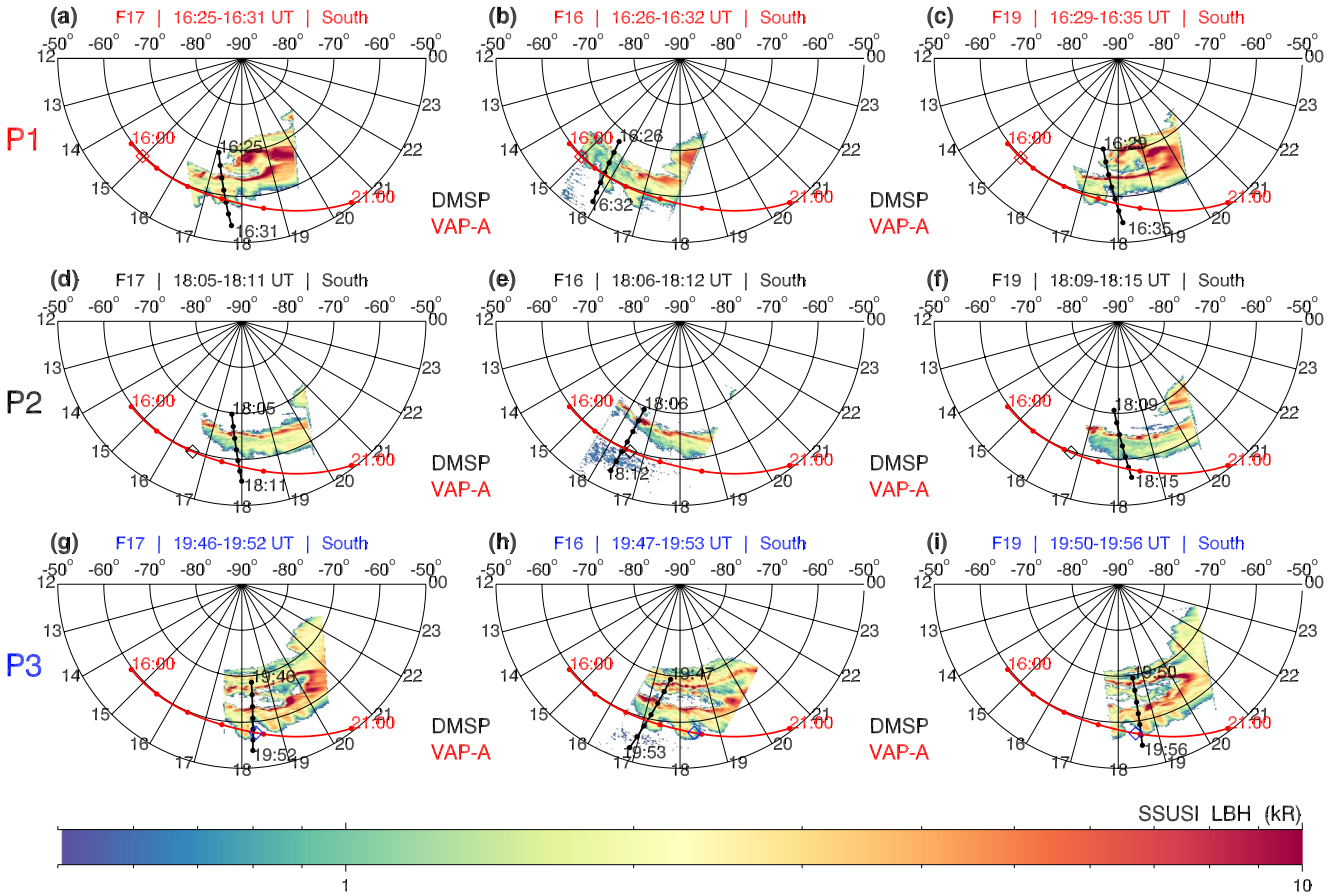

Figure 1. Giant aurora undulations in the south hemisphere shot by DMSP F17, F16, and F19 satellites. The trajectories of DMSP (black) and VAP-A (red) satellites are overlapped with 1 min and 1 hr intervals, respectively. The aurora imaging times are labeled on the top of each panel. The footprint trajectory of VAP-A during 16:00–21:00 UT is obtained by the Tsyganenko 96 (T96) magnetic field model projection, with diamonds representing the VAP-A footprint location at moments of each aurora imaging. P1 (16:30–17:30 UT), P2 (18:00–18:50 UT), and P3 (19:30–20:15 UT) mark three periods of distinct magnetospheric particles and waves signatures by VAP-A, which can be detailed in the context. The auroras on the same row were shot within a 10 min period, separately falling into the P1, P2, and P3 periods.

GUs were larger and brighter at 16:25–16:35 UT, subsequently shrank and weakened during 18:05–18:15 UT, and finally again amplified in size and luminosity at 19:46–19:56 UT. The three-stage evolution pattern, termed as strong-weak-strong, during 16:00–21:00 UT theoretically can reflect three different PSWs at the conjugate magnetospheric source region during three corresponding time intervals, when considering the GUs acting as the ionospheric manifestation of the PSW (He et al., 2020; Zhou et al., 2022).

The ionospheric footprint of VAP-A during 16:00–21:00 UT is superposed as the red line in each panel, with a diamond marking the exact position of VAP-A footprint at the time of each auroral observation. It is noteworthy that part of the VAP-A orbit, highlighted by the footprints (diamonds), overlaps with the observed GUs in Figures 1b and 1g–1i, while other sections of the orbit are located 1.5 hr (Figure 1a), 2 hr (Figure 1c) and 1 hr (Figures 1d–1f) MLT westward of the sunward edge of the imaged GUs. For the latter situation, it is necessary to identify the accurate time when the footprint of VAP-A encounters a train of detectable GUs/PSW. During this event, the westward/sunward propagating speed of the GUs/PSWs was calculated to be 0.85°/min (Zhou, He, Zhang, et al., 2024), slightly larger than previously reported events (He et al., 2020; Henderson et al., 2010). Additionally, the VAP-A traveled anti-sunward from the afternoon sector with an azimuthal velocity of ∼1 hr MLT per hour, that is, 0.25°/min, to the dusk sector during 16:00–20:00 UT. As a result, the GUs and VAP-A satellite traveled toward each other in the total azimuthal velocity of ∼1.1°/min for the azimuthal distance of 1.5 hr/22.5°, 2 hr/30° and 1 hr/15° mentioned above. Correspondingly, the traveling times are separately calculated to be 20 min (16:45–16:51 UT in Figure 1a), 27 min (16:56–17:02 UT in Figure 1c) and 14 min (18:19–18:25 UT, 18:20–18:26 UT, and 18:23–18:29 UT in Figure 1d–1f), after which the VAP-A would go through a

train of magnetospheric PSW. Combined with the observed three-stage signatures of GUs, the VAP-A is estimated to encounter the strong GUs at 16:26–17:02 UT (termed as GU1), weak GUs at 18:19–18:29 UT (GU2), and again strong GUs at 19:46–19:56 UT (GU3).

2.2. Plasmapause Surface Waves Modulating Time Domain Structures

At the conjugate magnetospheric location, VAP-A traveled azimuthally from the afternoon to pre-midnight sector near the plasmapause at 16:00–21:00 UT, detecting in situ wave and plasma environment of the PSW in Figure 2. From 16:00 to 21:00 UT, the radial, azimuthal and parallel magnetic field and radial and azimuthal electric field recurrently oscillate within the frequency of 0.7–2 mHz (Figures 2b and 2c), generally in accordance with the typical frequency of PSWs (e.g., Feng et al., 2023; He et al., 2020; Zhou, He, Archer, et al., 2024). Meanwhile, the energy and count of thermal electron and energetic proton, O^+ and He^+ ion synchronously suffer the same periodic modulations (Figures 2d–2g). The total electron density is observed to be periodically disturbed (Figures 2h and 2i). It is noteworthy that a segment of total electron density with the most intense disturbance at 17:00–18:37 UT has a stable anti-phase relationship with particles' energy and count, indicative of the periodic intrusion of plasmaspheric cold electron by magnetospheric energetic electron and ions (He et al., 2020; Zhou, He, Archer, et al., 2024). However, the total electron density at 16:30–17:00 UT and 19:30–20:15 UT is only gently disturbed. Regardless of it, the existence of magnetospheric PSWs is unambiguously confirmed by combing the conjugate GUs and the modulation of in situ magnetic and electric fields, energetic particles and cold electron.

Generally, the intensity of PSWs can be divided into three stages including P1 for 16:30–17:30 UT, P2 for 18:00–18:50 UT and P3 for 19:30–20:15 UT. At P1, the thermal electron intensely fluctuates in the higher energy range up to 400 eV and more particle number exceeding 10^3 count/s, accompanied by stronger magnetic field disturbances with a maximal amplitude of ∼30 nT. Meanwhile, the fluctuation of energetic proton and O^+ ion also shows more particle count. Hence, the PSW at P1, termed as PSW1 hereafter, can be classified as an intense PSW. At P2, thermal electron displays evident fluctuations mainly in the energy range less than 120 eV, and energetic ions also show fluctuations of smaller count mostly less than $10^{1.2}$ count/s. Correspondingly, the gentle magnetic field disturbance is less than 10 nT. We can classify the PSW at P2 to be a weak PSW, that is, PSW2. Similarly, at P3, the PSW3 manifests as the strongest PSW characterized by the highest electron modulation energy up to ∼1 keV and number of 10^3 count/s, the most ion modulation number of 10^2 count/s and the strongest magnetic disturbance exceeding 30 nT. The intense (16:30–17:30 UT)-weak (18:00–18:50 UT)-intense (19:30–20:15) three-stage PSWs observed near the dusk plasmapause are strikingly accordance with the aforementioned strong (16:26–17:02 UT)-weak (18:19–18:29 UT)-strong (19:46–19:56 UT) GUs in the conjugate ionospheric region, with three durations of the latter separately falling into those of the former.

Importantly, the distinction of the PSW1, PSW2 and PSW3 are attributed to the temporal effect of ∼100 min (a DMSP orbit period) but not the spatial (MLT) effect. For the first reason, the corresponding wide-field GUs confirm that the classification on the scale and intensity of GU1, GU2 and GU3 is hardly influenced by the different MLT. Even though the GU3 in Figures 1j and 1i slightly decrease as the increasing of MLT, the smallest sawtooth substructure at the nightward edge of GUs still own a bigger amplitude (∼3° MLAT) than GU2 (<2° MLAT). Thus, the nearly MLT-independent GUs can reflect nearly MLT-independent PSWs. For the second reason, if we apply the spatial evolution effect to this event, it is hard to explain the PSW intensification again at the afternoon sector (15.4–16.1 hr MLT) based on the pre-midnight excitement of PSWs by substorm energetic particles injections (Hao et al., 2023; He et al., 2020; Zhou, He, Archer, et al., 2024; Zhou et al., 2021). For the last reason, PSW1, PSW2 and PSW3 with such a long-time interval of ∼100 min are under different substorm conditions with AE index of 1,500–2,800 nT, 800 nT, and 1,000–1,400 nT (Figure 2a), respectively, which can provide different energy sources to generate PSWs of different intensity levels during this three periods.

Besides the ULF modulations, there also exist VLF wave modes with their frequency, wave normal angle and ellipticity signatures shown in Figures 2j–2m. During 17:00–18:15 UT, plasmaspheric hiss wave recurrently appears in the frequency range from 20 Hz to $0.1f_{ce}$ with the field-aligned propagation (WNA: 0–10°) and the right-handed circular polarization (ellipticity: >0.7) (e.g., Li et al., 2019; Liu et al., 2019; Zhu et al., 2015). The hiss wave periodically appears at electron density peaks, indicating the strong modulation effect by periodically disturbed total electron density in the PSW frequency (Hao et al., 2023; Koons, 1989; Malaspina et al., 2018; Moullard et al., 2002). On one hand, however, the hiss wave typically contributes to the precipitation of radiation belt electron and hardly has effect on the cold electrons herein (e.g., Agapitov et al., 2020; Meredith et al., 2004;

10.1029/2024GL111782

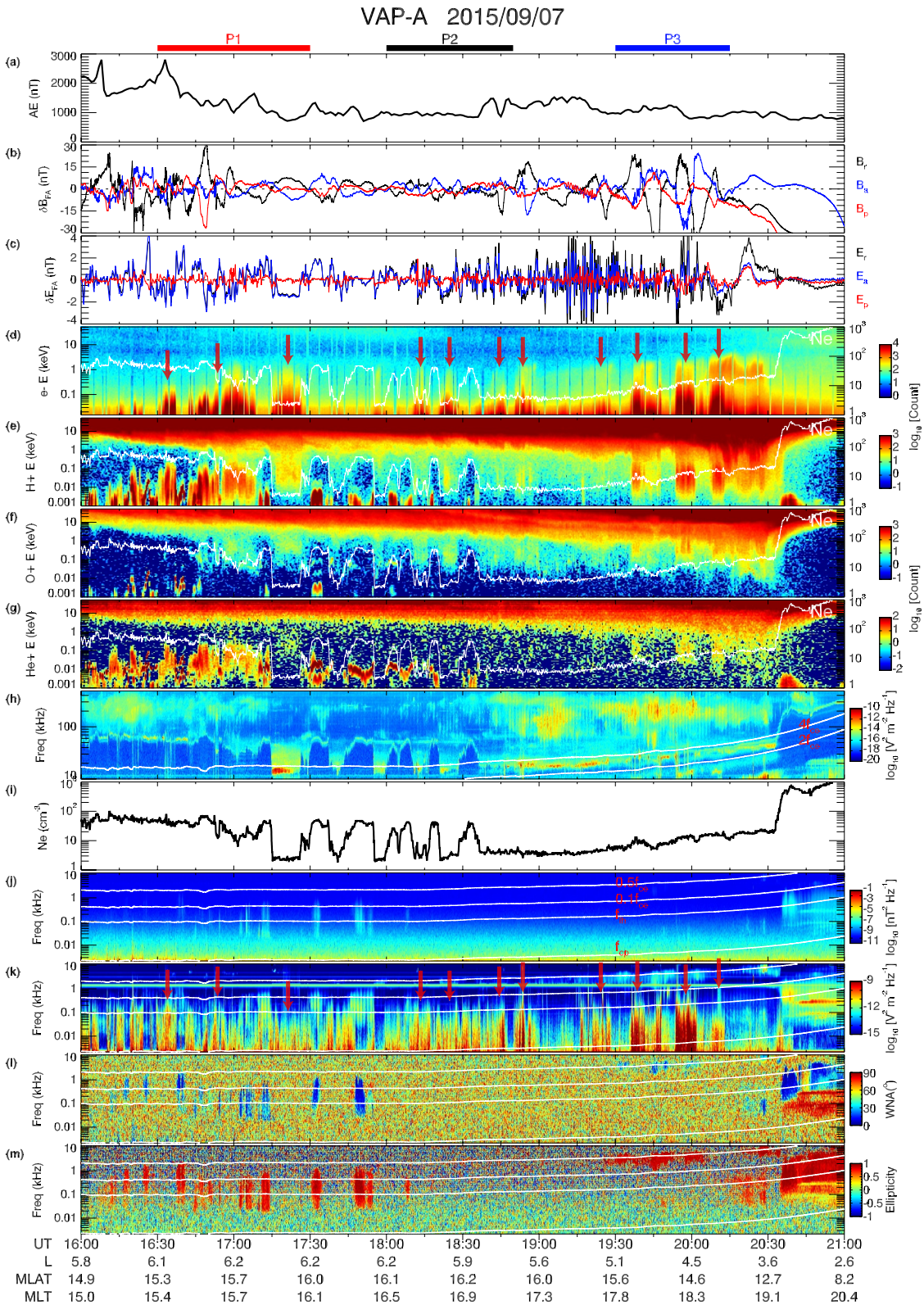

Figure 2.

Thorne et al., 1973). On the other hand, no hiss wave is observed during P3 when the strongest PSW occurs. Hence, the hiss wave is modulated by intense density variations rather than the PSW itself in this event. Similarly, the weak lower-band chorus (ECH) wave with frequency of 0.1–0.5 f_{ce} (2–4 f_{ce}) only appears locally at 19:30–20:05 UT (18:52–20:35 UT) in Figure 2k (2 hr) and does not obey the periodical modulation of the PSW and particles. Further, no evident electromagnetic ion cyclotron (EMIC) wave (not shown here) is detected.

Alternatively, broadband electrostatic fluctuations periodically enhance at 16:15–20:15 UT in Figure 2k, including nonlinear electrostatic structures typically termed as time domain structures (TDSs) (e.g., Ergun et al., 2015; Khazanov et al., 2021; Shen et al., 2020). As marked by red vertical arrows in Figures 2d and 2k, the TDSs generally correspond to the periodical enhancement of energy and count of thermal electron in the PSW frequency, in accordance with that TDSs can accelerate and scatter plasma sheet electrons, contributing to the diffuse aurora confirmed in previous research (e.g., Mozer et al., 2017; Shen et al., 2020; Vasko et al., 2018). Therefore, it is the TDSs rather than chorus and ECH waves that are periodically modulated by the PSWs.

2.3. Pitch-Angle Distribution of Modulated Particles

Figure 3 displays the PA distribution of thermal electron and proton at typical energy channels in detail. For the thermal electron and energetic proton modulated by the PSW, their PA distributions generally display the periodical bidirectional signature, that is, 0° and 180°. Specifically, this kind of bidirectional PA distribution has appeared in the 15.0 eV energy channel (Figure 3b), above which the bidirectional signatures become more distinct (Figures 3c and 3d). Up to the energy channel of ∼235.5 eV (Figure 3e), the bidirectional particle distribution nearly disappears at P2 for the weak PSW2 but is still evident at P1 and P3 for the intense PSW1 and PSW3. Actually, at P1 (PSW1) and P3 (PSW3), the energy channel of bidirectional distribution persists up to ∼933.3 eV (Figure 3f), close to 1 keV. Besides, the electron total fluxes during one PSW period (termed as one-period flux) near the 0° and 180° PA at P1 and P3 are much larger than that at P2 for the periodical bidirectional thermal electron.

Similar to the thermal electron, energetic proton also displays the bidirectional distribution of PA, which begins from the energy of ∼45.7 eV in Figure 3i, nearly disappears up to the energy of ∼7.1 keV at P1 and P2 in Figure 3k, but is still partly observed at the proton energy up to 51.8 keV at P3 in Figure 3l. Besides, the proton one-period fluxes near the 0° and 180° PA at P1 and P3 are much larger than that at P2. Although the count and temporal resolution are low, the O^+ and He^+ ions also show the similar bidirectional PA distribution to some extent.

Although the VAP-A is unable to resolve the small loss cone angle on the magnetic equator, other observational evidence can still establish the relation of bidirectional distribution, PA scattering, precipitation and aurora. First, combined with the above ionospheric observations, the strong bidirectional distribution of magnetospheric thermal electron with higher energy and larger one-period flux at P1 and P3 (more intense PSW1 and PSW3) corresponds to larger and brighter GU1 and GU3 at the conjugate ionosphere. In contrast, the weak bidirectional distribution at P2 (weak PSW2) matches smaller and dimmer GU2. Thus, the positive correlation between bidirectional distribution and aurora is established. Second, the periodical bidirectional distributions of <1 keV thermal electron and 45.7 eV–51.8 keV energetic ions are accompanied by TDSs, which has been confirmed to be associated with the formation of highly field-aligned electron distributions (Mozer et al., 2015, 2017) and to cause strong diffusion to fill the loss cone of low-energy (<1 keV) plasma sheet electron, finally contributing to diffuse auroras (e.g., Khazanov et al., 2021; Shen et al., 2020, 2024). Accordingly, the relation of bidirectional distribution, PA scattering and GUs via the TDSs is supported by previous theoretical and observational research. Lastly, DMSP satellites detect simultaneous <1 keV thermal electron and ion precipitation and energetic ion

Figure 2. In situ waves and particles characteristics during 16:00–21:00 UT measured by VAP-A satellite. (a) AE index; (b–c) ULF wave magnetic and electric field detrended by the 30 min smooth average; (d–g) energy spectrograms of omnidirectional electron, proton (H^+), oxygen ion (O^+) and helium ion (He^+); (h–i) high frequency spectrogram of electric field and electron density inferred from the upper hybrid resonance frequency; (j–m) frequency-time spectrograms of magnetic and electric spectral density, wave normal angle (WNA), and ellipticity. The electron density in panel (i) is also superimposed on panels (d–g) as white curves. The white lines denote $4f_{ce}$, $2f_{ce}$ in panel (h), and $0.5f_{ce}$, $0.1f_{ce}$, f_{lh}, f_{cp} in panels (j–m), where f_{ce} (f_{cp}) is electron (proton) cyclotron frequency and f_{lh} is lower hybrid resonance frequency. Three thick lines labeled as P1 (16:30–17:30 UT; red), P2 (18:00–18:50 UT; black), and P3 (19:30–20:15 UT; blue) highlight three periods of different magnetospheric particles and waves signatures. Red vertical arrows in panels (d) and (k) mark the correspondence between TDSs and thermal electron enhancement. Subscript: p-parallel; r-radial; a-azimuthal.

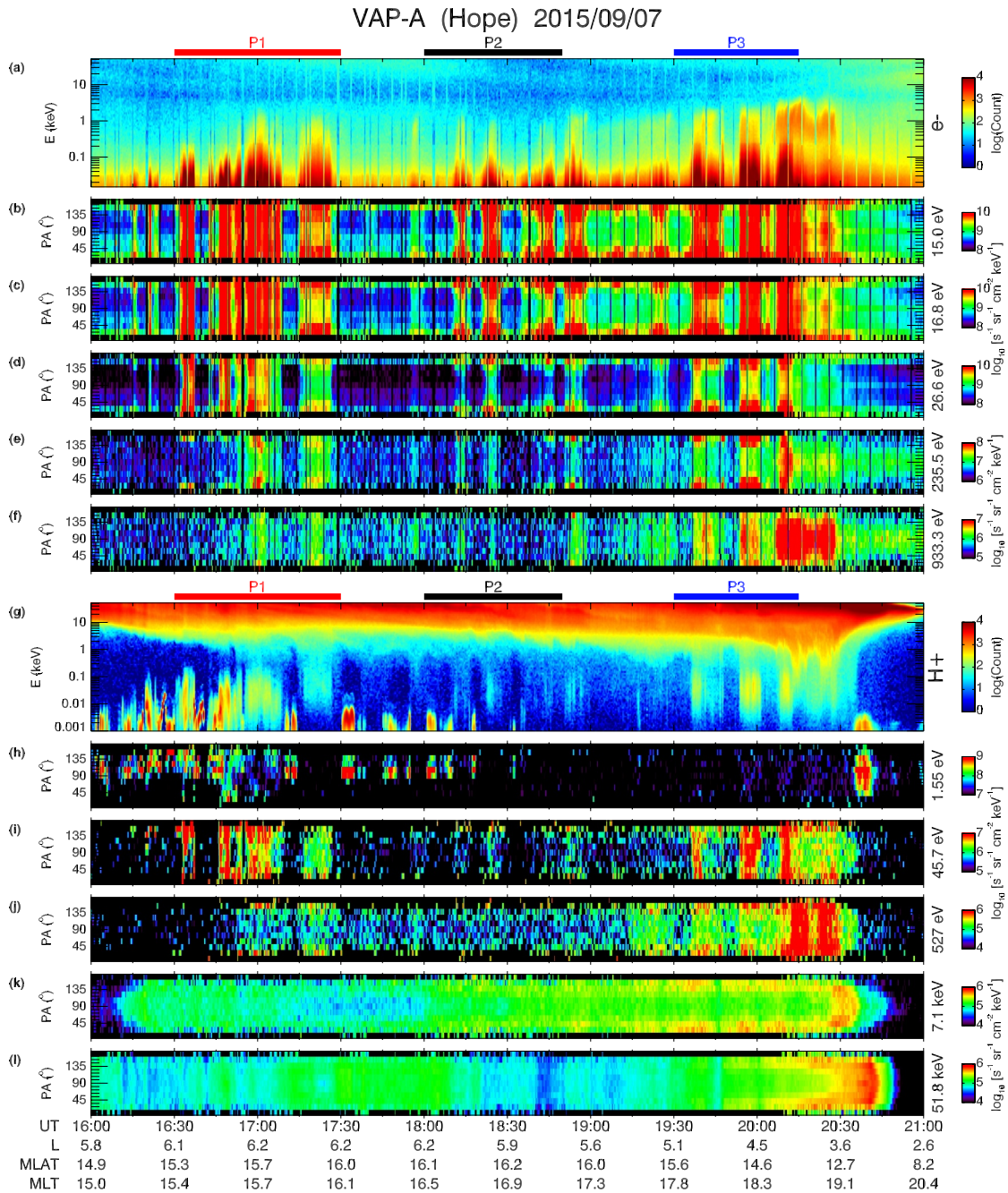

Figure 3. Pitch-angle distribution of thermal electron and proton at typical energy channels. (a) Energy spectrograms of omnidirectional electron; (b–f) PA distribution of electron at 15.0, 16.8, 26.6, 235.5, and 933.3 eV; (g) energy spectrograms of omnidirectional proton; (h–l) PA distribution of proton at 1.55, 45.7, 527, 7.1, and 51.8 keV. The same three thick lines P1 (red), P2 (black), and P3 (blue) as Figures 1 and 2 highlight three periods of different magnetospheric particles and waves signatures.

precipitation up to dozens of keV over ionospheric GUs in the same GUs event, as displayed in Figures 1–4 in Zhou, He, Zhang, et al. (2024), hence verifying the close correlation of bidirectional distribution, precipitation and GUs.

Therefore, the PSWs can modulate the intensity of TDSs to scatter and precipitate the thermal electron and ion and energetic ions to form GUs, in contrast with previous prediction of the PSW modulating chorus or ECH waves to precipitate particles (Hao et al., 2023; He et al., 2020; Zhou, He, Zhang, et al., 2024).

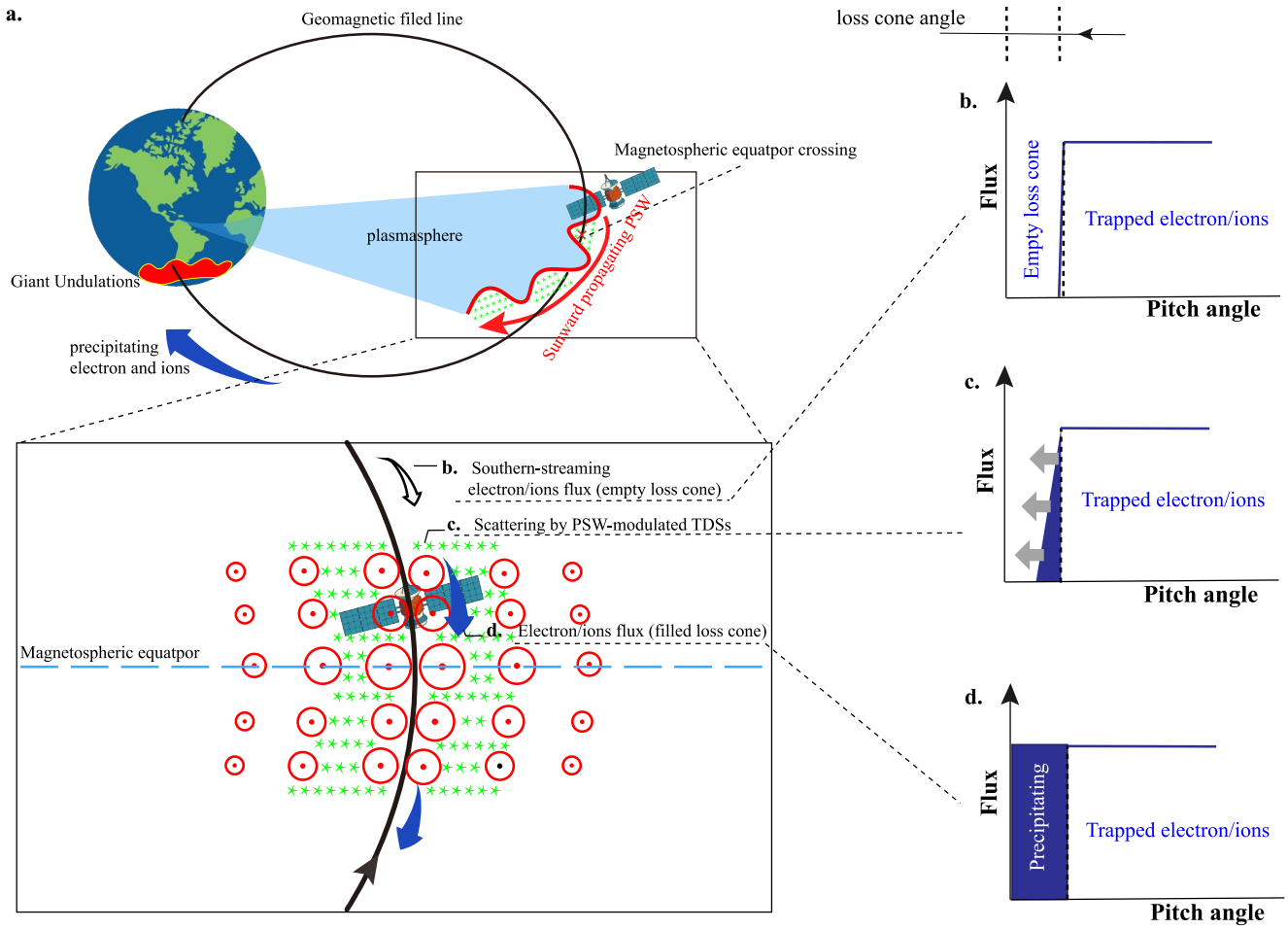

Figure 4. Schematic of electron and ions scattering by the PSW-modulated TDSs, resulting in GUs. (a) The open/filled blue arrow represents southward streaming electrons and ions with the empty/filled loss cone (b)/(d) before/after the PSWs-modulated TDSs interact with them (c) (pitch-angle scattering by waves). The spacecraft location is denoted by a black filled circle. (b–d) The evolution of the electron PAD. The red symbols⊙represent the sunward propagating PSWs with the size of circles denoting the intensity of PSWs. And green asterisks * denote the TDSs modulated by PSWs.

2.4. A Schematic Description

Figure 4 shows a schematic of electron and ions scattering by the PSW-modulated TDSs, resulting in GUs. After the PSWs are excited at the post-dusk sector (18–19 MLT; Zhou, He, Archer, et al., 2024; Zhou et al., 2021), they propagate sunward (red arrow and⊙in Figure 4a) near the wavy plasmapause and modulate the TDSs intensity (asterisks in Figure 4a), which interact with bouncing-drifting electrons and ions. As these electrons and ions are scattered by the electric fields of TDSs, some of them become nearly parallel to the magnetic field, subsequently falling into the empty loss cone (blue open arrow in Figure 4a) and filling it (blue filled arrows in Figure 4a), and finally precipitating into the upper atmosphere to generate GUs (top left in Figure 4a).

3. Summary and Conclusion

In this letter, we have provided the observational evidence of giant aurora undulations being driven by the pitch-angle scattering of thermal electron by the PSW-modulated TDSs, via the conjugate magnetospheric and ionospheric satellites, which plugs the gap between the PSW and GUs to some extent. The specific new findings are listed as follows.

1. GUs are lighted by the pitch-angle scatter of <1 keV thermal electron and ions and energetic ions with energy up to dozens of keV.

2. The total fluxes during one PSW period and energy of scattered electron and ions determine the size and luminosity of ionospheric GUs.
3. PSWs can periodically modulate TDSs, which scatter and precipitate thermal electron to form GUs, in contrast with previous prediction of the PSW modulating chorus or ECH waves to precipitate particles.

Despite the significant progress made in this letter, we would like to emphasize that the fundamental physical mechanisms underlying the observed simultaneous pitch-angle interactions between PSW-modulated TDSs, thermal electrons, and multiple species of energetic ions remain unknown and warrant further investigation in the future.

Data Availability Statement

All kinds of satellites data are publicly available at Zhou (2024). The SPEDAS software used for wave analysis is publicly described at Angelopoulos et al. (2019).

Acknowledgments
This work was supported by the National Natural Science Foundation of China (42222408, 42441809), the National Key R&D Program of China (2021YFA0718600) and the Youth Innovation Promotion Association of the Chinese Academy of Sciences (No. Y2021027). We would like to thank the entire VAP and DMSP team for providing data access and support. Special thanks to Funsten H. O., Kletzing, C. A. and Spence, H. E. for their contributions in making available data from HOPE, EMFISIS and ECT, respectively.

References

Agapitov, O., Glassmeier, K. H., Plaschke, F., Auster, H., Constantinescu, D., Angelopoulos, V., et al. (2009). Surface waves and field line resonances: A THEMIS case study. *Journal of Geophysical Research*, *114*(A1), A00C27. https://doi.org/10.1029/2008JA013553

Agapitov, O., Mourenas, D., Artemyev, A., Claudepierre, S. G., Hospodarsky, G., & Bonnell, J. W. (2020). Lifetimes of relativistic electrons as determined from plasmaspheric hiss scattering rates statistics: Effects of ωpe/Ωce and wave frequency dependence on geomagnetic activity. *Geophysical Research Letters*, *47*(13), e2020GL088052. https://doi.org/10.1029/2020GL088052

Angelopoulos, V., Cruce, P., Drozdov, A., Grimes, E. W., Hatzigeorgiu, N., King, D. A., et al. (2019). The space physics environment data analysis system (SPEDAS). *Space Science Reviews*, *215*(1), 9. https://doi.org/10.1007/s11214-018-0576-4

Archer, M. O., Hartinger, M. D., Rastätter, L., Southwood, D. J., Heyns, M., Eggington, J. W. B., et al. (2023). Auroral, ionospheric and ground magnetic signatures of magnetopause surface modes. *Journal of Geophysical Research: Space Physics*, *128*(3), e2022JA031081. https://doi.org/10.1029/2022JA031081

Archer, M. O., Hietala, H., Hartinger, M. D., Plaschke, F., & Angelopoulos, V. (2019). Direct observations of a surface eigenmode of the dayside magnetopause. *Nature Communications*, *10*(1), 615. https://doi.org/10.1038/s41467-018-08134-5

Chen, L., & Hasegawa, A. (1974). A theory of long-period magnetic pulsations: 2. Impulse excitation of surface eigenmode. *Journal of Geophysical Research*, *79*(7), 1033–1037. https://doi.org/10.1029/JA079i007p01033

Ergun, R. E., Goodrich, K. A., Stawarz, J. E., Andersson, L., & Angelopoulos, V. (2015). Large-amplitude electric fields associated with bursty bulk flow braking in the Earth's plasma sheet. *Journal of Geophysical Research: Space Physics*, *120*(3), 1832–1844. https://doi.org/10.1002/2014JA020165

Feng, Z.-J., Ren, J., Zong, Q.-G., Xiang, T.-Y., & Ai, X.-Y. (2023). Statistical properties of long-period plasmapause surface waves from Van Allen Probes observations. *Journal of Geophysical Research: Space Physics*, *128*(7), e2023JA031572. https://doi.org/10.1029/2023JA031572

Florinski, V., Zank, G. P., & Pogorelov, N. V. (2005). Heliopause stability in the presence of neutral atoms: Rayleigh-taylor dispersion analysis and axisymmetric MHD simulations. *Journal of Geophysical Research*, *110*(A7), A07104. https://doi.org/10.1029/2004JA010879

Funsten, H. O., Skoug, R. M., Guthrie, A. A., MacDonald, E. A., Baldonado, J. R., Harper, R. W., et al. (2013). Helium, oxygen, proton, and electron (HOPE) mass spectrometer for the radiation belt storm probes mission. *Space Science Reviews*, *179*(1–4), 423–484. https://doi.org/10.1007/s11214-013-9968-7

Hao, Y. X., Zong, Q.-G., Yue, C., Zhou, X., Zhang, H., Pu, Z. Y., & Shprits, Y. Y. (2023). Plasmapause surface waves triggered by substorms. *Journal of Geophysical Research: Space Physics*, *128*(6), e2021JA029962. https://doi.org/10.1029/2021JA029962

Hartinger, M. D., Plaschke, F., Archer, M. O., Welling, D. T., Moldwin, M. B., & Ridley, A. (2015). The global structure and time evolution of dayside magnetopause surface eigenmodes. *Geophysical Research Letters*, *42*(8), 2594–2602. https://doi.org/10.1002/2015GL063623

Hasegawa, H., Fujimoto, M., Phan, T.-D., Rème, H., Balogh, A., Dunlop, M. W., et al. (2004). Transport of solar wind into Earth's magnetosphere through rolled-up Kelvin–Helmholtz vortices. *Nature*, *430*(7001), 755–758. https://doi.org/10.1038/nature02799

He, F., Guo, R.-L., Dunn, W. R., Yao, Z. H., Zhang, H. S., Hao, Y. X., et al. (2020). Plasmapause surface wave oscillates the magnetosphere and diffuse aurora. *Nature Communications*, *11*(1), 1668. https://doi.org/10.1038/s41467-020-15506-3

Henderson, M. G., Donovan, E. F., Foster, J. C., Mann, I. R., Immel, T. J., Mende, S. B., & Sigwarth, J. B. (2010). Start-to-end global imaging of a sunward propagating, SAPS-associated giant undulation event. *Journal of Geophysical Research*, *115*(A4), A04210. https://doi.org/10.1029/2009ja014106

Khazanov, G. V., Shen, Y., Vasko, I. Y., Artemyev, A. V., & Chu, M. (2021). Magnetosphere-ionosphere coupling of precipitated electrons in diffuse aurora driven by time domain structures. *Geophysical Research Letters*, *48*(10), e2021GL092655. https://doi.org/10.1029/2021GL092655

Kletzing, C. A., Kurth, W. S., Acuna, M., MacDowall, R. J., Torbert, R. B., Averkamp, T., et al. (2013). The electric and magnetic field instrument suite and integrated science (EMFISIS) on RBSP. *Space Science Reviews*, *179*(1–4), 127–181. https://doi.org/10.1007/s11214-013-9993-6

Koons, H. C. (1989). Observations of large-amplitude, whistler mode wave ducts in the outer plasmasphere. *Journal of Geophysical Research*, *94*(A11), 15393–15397. https://doi.org/10.1029/JA094iA11p15393

Kozyreva, O., Pilipenko, V., Lorentzen, D., Baddeley, L., & Hartinger, M. (2019). Transient oscillations near the dayside open-closed boundary: Evidence of magnetopause surface mode? *Journal of Geophysical Research: Space Physics*, *124*(11), 9058–9074. https://doi.org/10.1029/2018JA025

Lewis, W. S., Burch, J. L., Goldstein, J., Horton, W., Perez, J. C., Frey, H. U., & Anderson, P. C. (2005). Duskside auroral undulations observed by IMAGE and their possible association with large-scale structures on the inner edge of the electron plasma sheet. *Geophysical Research Letters*, *32*(24), 348–362. https://doi.org/10.1029/2005GL024390

Li, B., Habbal, S. R., & Chen, Y. (2013). The period ratio for standing kink and sausage modes in solar structures with siphon flow. I. magnetized slabs. *The Astrophysical Journal*, *767*(2), 169–184. https://doi.org/10.1088/0004-637X/767/2/169

Li, T., Li, W., Tang, B., Khotyaintsev, Y. V., Graham, D. B., Ardakani, A., et al. (2023). Kelvin-Helmholtz waves and magnetic reconnection at the Earth's magnetopause under southward interplanetary magnetic field. *Geophysical Research Letters*, *50*(20), e2023GL105539. https://doi.org/10.1029/2023GL105539

Li, W., Shen, X.-C., Ma, Q., Capannolo, L., Shi, R., Redmon, R. J., et al. (2019). Quantification of energetic Electron precipitation driven by plume whistler mode waves, Plasmaspheric hiss, and exohiss. *Geophysical Research Letters*, *46*(7), 3615–3624. https://doi.org/10.1029/2019GL082095

Liu, N., Su, Z., Gao, Z., Zheng, H., Wang, Y., & Wang, S. (2019). Magnetospheric chorus, exohiss, and magnetosonic emissions simultaneously modulated by fundamental toroidal standing Alfvén waves following solar wind dynamic pressure fluctuations. *Geophysical Research Letters*, *46*(4), 1900–1910. https://doi.org/10.1029/2018GL081500

Lui, A. T. Y., Meng, C. I., & Ismail, S. (1982). Large amplitude undulations on the equatorward boundary of the diffuse aurora. *Journal of Geophysical Research*, *87*(A4), 2385–2400. https://doi.org/10.1029/JA087iA04p02385

Malaspina, D. M., Ripoll, J.-F., Chu, X., Hospodarsky, G., & Wygant, J. (2018). Variation in plasmaspheric hiss wave power with plasma density. *Geophysical Research Letters*, *45*(18), 9417–9426. https://doi.org/10.1029/2018GL078564

Mann, I. R., Wright, A. N., Mills, K. J., & Nakariakov, V. M. (1999). Excitation of magnetospheric waveguide modes by magnetosheath flows. *Journal of Geophysical Research*, *104*(A1), 333–353. https://doi.org/10.1029/1998JA900026

Meredith, N. P., Horne, R. B., Thorne, R. M., Summers, D., & Anderson, R. R. (2004). Substorm dependence of plasmaspheric hiss. *Journal of Geophysical Research*, *109*(A6), A06209. https://doi.org/10.1029/2004JA010387

Moullard, O., Masson, A., Laakso, H., Parrot, M., Décréau, P., Santolik, O., & Andre, M. (2002). Density modulated whistler mode emissions observed near the plasmapause. *Geophysical Research Letters*, *29*(20), 1975. https://doi.org/10.1029/2002GL015101

Mozer, F. S., Agapitov, O., Artemyev, A., Drake, J. F., Krasnoselskikh, V., Lejosne, S., & Vasko, I. (2015). Time domain structures: What and where they are, what they do, and how they are made. *Geophysical Research Letters*, *42*(10), 3627–3638. https://doi.org/10.1002/2015GL063946

Mozer, F. S., Agapitov, O. V., Hull, A., Lejosne, S., & Vasko, I. Y. (2017). Pulsating auroras produced by interactions of electrons and time domain structures. *Journal of Geophysical Research: Space Physics*, *122*(8), 8604–8616. https://doi.org/10.1002/2017JA024223

Nishitani, N., Hough, G., & Scourfield, M. W. J. (1994). Spatial and temporal characteristics of giant undulations. *Geophysical Research Letters*, *21*(24), 2673–2676. https://doi.org/10.1029/94gl02240

Paxton, L. J., Morrison, D., Zhang, Y. L., Kil, H., Wolven, B., Ogorzalek, B. S., et al. (2002). Validation of remote sensing products produced by the special sensor ultraviolet scanning imager (SSUSI): A far UV-imaging spectrograph on DMSPF-16. *Proceedings of SPIE*, *4485*, 338–348. https://doi.org/10.1117/12.454268

Plaschke, F., & Glassmeier, K. H. (2011). Properties of standing Kruskal-Schwarzschild-modes at the magnetopause. *Annales Geophysicae*, *29*(10), 1793–1807. https://doi.org/10.5194/angeo-29-1793-2011

Pu, Z.-Y., & Kivelson, M. G. (1983). Kelvin-Helmholtz instability at the magnetopause: Solution for compressible plasmas. *Journal of Geophysical Research*, *88*(A2), 841–852. https://doi.org/10.1029/ja088ia02p00841

Rae, I. J., Donovan, E. F., Mann, I. R., Fenrich, F. R., Watt, C. E. J., Milling, D. K., et al. (2005). Evolution and characteristics of global Pc5 ULF waves during a high solar wind speed interval. *Journal of Geophysical Research*, *110*(A12), A12211. https://doi.org/10.1029/2005ja011007

Shen, Y., Artemyev, A., Zhang, X.-J., Vasko, I. Y., Runov, A., Angelopoulos, V., & Knudsen, D. (2020). Potential evidence of low-energy electron scattering and ionospheric precipitation by time domain structures. *Geophysical Research Letters*, *47*(16), e2020GL089138. https://doi.org/10.1029/2020GL089138

Shen, Y., Liang, J., Artemyev, A., Angelopoulos, V., Ma, Q., Lyons, L., et al. (2024). Red line diffuse-like aurora driven by time domain structures associated with braking magnetotail flow bursts. *Geophysical Research Letters*, *51*(10), e2024GL109000. https://doi.org/10.1029/2024GL109000

Stehle, R., & Spruit, H. C. (1999). Hydrodynamics of accretion discs of variable thickness. *Monthly Notices of the Royal Astronomical Society*, *304*(3), 674–686. https://doi.org/10.1046/j.1365-8711.1999.02390.x

Thorne, R. M., Smith, E. J., Burton, R. K., & Holzer, R. E. (1973). Plasmaspheric hiss. *Journal of Geophysical Research*, *78*(10), 1581–1596. https://doi.org/10.1029/JA078i010p01581

Vasko, I. Y., Krasnoselskikh, V. V., Mozer, F. S., & Artemyev, A. V. (2018). Scattering by the broadband electrostatic turbulence in the space plasma. *Physics of Plasmas*, *25*(7), 072–903. https://doi.org/10.1063/1.5039687

Wygant, J. R., Bonnell, J. W., Goetz, K., Ergun, R. E., Mozer, F. S., Bale, S. D., et al. (2013). The electric field and waves instruments on the radiation belt storm probes mission. *Space Science Reviews*, *179*(1–4), 183–220. https://doi.org/10.1007/s11214-013-0013-7

Xiao, C., He, F., Shi, Q., Liu, W., Tian, A., Guo, R., et al. (2023). Evidence for lunar tide effects in Earth's plasmasphere. *Nature Physics*, *19*(4), 486–491. https://doi.org/10.1038/s41567-022-01882-8

Zhang, Y., Paxton, L. J., Morrison, D., Lui, A. T. Y., Kil, H., Wolven, B., et al. (2005). Undulations on the equatorward edge of the diffuse proton aurora: TIMED/GUVI observations. *Journal of Geophysical Research*, *110*(A8), A08211. https://doi.org/10.1029/2004JA010668

Zhou, Y.-J. (2024). Data for article "giant undulations driven by pitch-angle scattering of plasmapause surface wave" [Dataset]. *figshare*. https://doi.org/10.6084/m9.figshare.26309671.v1

Zhou, Y.-J., He, F., Archer, M. O., Zhang, X., Hao, Y. X., Yao, Z., et al. (2024). Spatial evolution characteristics of plasmapause surface wave during a geomagnetic storm on 16 July 2017. *Geophysical Research Letters*, *51*(8), e2024GL109371. https://doi.org/10.1029/2024GL109371

Zhou, Y.-J., He, F., Yao, Z.-H., Wei, Y., Zhang, X., & Zhang, Y. (2022). Correlations between giant undulations and plasmapause configurations. *Geophysical Research Letters*, *49*(13), e2022GL098627. https://doi.org/10.1029/2022GL098627

Zhou, Y.-J., He, F., Zhang, X.-X., Archer, M. O., Lin, Y., Ma, H., et al. (2023). A radial standing Pc5-6 wave and its energy coupling with field line resonance within the dusk-sector magnetosphere. *Journal of Geophysical Research: Space Physics*, *128*(10), e2023JA031835. https://doi.org/10.1029/2023JA031835

Zhou, Y.-J., He, F., Zhang, X.-X., Yao, Z., Wei, Y., & Zhang, Y. (2021). Statistical characteristics of giant undulations during geomagnetic storms. *Geophysical Research Letters*, *48*(13), e2021GL093098. https://doi.org/10.1029/2021GL093098

Zhou, Y.-J., He, F., Zhang, X.-X., Zhang, Y., Liu, L., Yao, Z., et al. (2024). Special particle precipitation signatures over giant auroral undulations during the 7 September 2015 geomagnetic storm. *Geophysical Research Letters*, *51*(14), e2024GL109849. https://doi.org/10.1029/2024GL109849

Zhu, H., Su, Z., Xiao, F., Zheng, H., Wang, Y., Shen, C., et al. (2015). Plasmatrough exohiss waves observed by Van Allen Probes: Evidence for leakage from plasmasphere and resonant scattering of radiation belt electrons. *Geophysical Research Letters*, *42*(4), 1012–1019. https://doi.org/10.1002/2014GL062964